EXPLORATION OF QUANTUM OPTIMAL CONTROL

Undergraduate Senior Thesis

University of New Mexico

by

Julie Abigail Campos

May 14, 2020

ACKNOWLEDGEMENTS

EXPLORATION OF QUANTUM OPTIMAL CONTROL

ABSTRACT

In this senior thesis, we studied the resources used for controlling closed quantum systems of spins in the presence of electromagnetic fields through methods of quantum optimal control. By resources we mean physical quantities such as energy, time of control, and bandwidth of control waveforms which are modulated to achieve desirable state maps. Optimal control waveforms were found by numerically minimizing the infidelity which is the probability of not reaching a target state. The minimum time required to successfully implement a control, called the Quantum Speed Limit (QSL), was observed by plotting the best achieved infidelity versus the time allotted for control, T. It was observed that by increasing the bandwidth of the control waveform, the infidelity could be minimized for times greater than the QSL. In addition, for low bandwidths, the plots of infidelity versus total control time demonstrated behavior that can be interpreted as the effect of the topology of the Hilbert Space on the controllability. Results also showed that as the dimension of the Hilbert Space increased, longer times and bandwidths are required for successful optimal control as expected. Finally, an interesting feature of the control landscape for the control of a spin-1/2 particle is interpreted as what could be a general geometric property of dynamics implemented by unitary matrices from the Lie Group $SU(2)$.

CONTENTS

CHAPTER 1

INTRODUCTION

The nature of quantum mechanics allows us to create coherent superposition states that can interfere with each other. This enlarges the Hilbert space (state space) and opens up more possibilities of what can be done with a quantum system compared to what is possible with a classical system. Quantum technologies such as atom interferometry, atomic clocks, and quantum computing, take advantage of this [6, 18]. Reaching an arbitrary superposition state in state space or creating a unitary transformation is nontrivial since it depends on what interactions are available in the laboratory. Thus, it is important to determine what dynamics are possible with the Hamiltonian available. For example, if our goal is to drive a transition from one energy level to another or implement a quantum logic gate, we must determine if our physical system is controllable enough to achieve these goals. In addition to having a controllable system, one also needs to give the system sufficient time to evolve as we want. This sets a lower bound, called the Quantum Speed Limit (QSL), on the amount of time needed to control the system in a way that achieves desirable dynamics. We often want to control a quantum system near the QSL to avoid any unwanted corruption to quantum states, since superposition states are fragile and susceptible to decoherence. But sometimes it might not be in our best interest to do control at the QSL because, in general, as we decrease the time of control, higher bandwidths are required to implement rapidly changing control waveforms/functions. Quantum Optimal Control (QOC) is a strategy to help us find how we can reach our objective with limited resources. It searches for a control waveform that modulates the Hamiltonian in such a way that some cost function is optimized.

There is a trade-off between the limited resources that has not been explored extensively and is the focus of this thesis. In particular, we look how the availability of these resources affect each other for closed, controllable quantum systems of spins in the presence of electromagnetic fields. The trade-off changes with dimension of the Hilbert Space so our studies begin with the control of a spin-1/2 system in Chapter 2. Dynamics for this system are well understood by using concepts from quantum optics such as Rabi oscillations [9], so we take advantage of this and discuss it in this chapter. Substantial intuition is gained by studying the dynamics, which is helpful for us to understand why a control protocol is successful, and why it fails. Then, once the control problem is framed, controllability of the system is assessed and the implementation of optimal control is explained. Optimal control is used to achieve desired target states by finding control functions that maximize the probability of arriving at some target state. The control function is chosen to be a piecewise constant function that can be thought of as a pulse sequence. This pulse sequence is defined by pulses with different amplitudes but the same duration. Chapter 3 is the exploration of the optimal control of higher spin systems with piecewise constant control functions. The Hilbert Space of these systems is more complicated so the dynamics cannot be studied in the same intuitive way as with the spin-1/2, but there does exist a controllable Hamiltonian and its controllability is motivated [17].

1.1   What are Control and Optimal Control?

Control Theory is used in many subject fields to devise a control protocol which ensures that objectives are reached given some constraints. In both classical and

quantum control, it helps us answer the question of whether a system is controllable enough given the available interactions to achieve desired dynamics or not and also, how it can be controlled. There are two types of control protocols: open and closed loop controls. Open loop controls do not involve feedback since settings are predetermined without intermediate measurements. A closed loop control includes measurement and feedback during the process so that settings are modified until the desired outcome is achieved [23]. An example of closed-loop control in classical mechanics is the function of ventilators. The goal of ventilators is to assist when someone has trouble breathing so controlling the air that is transported to and from a patient is important. Oxygen level, air pressure and air volume have to be controlled accurately by the ventilator so these are measured continuously and to modify the settings as needed [4].

Within closed and open loop controls, one control strategy is optimal control. The question that is answered with optimal control is as follows. Assuming a quantum system can be controlled, what is the best way to control it and how well can it be controlled? The "best" way is one that minimizes a cost function. Optimal control problems are formulated mathematically such that there is a cost function to be optimized over chosen control parameters or waveforms, also called control functions [2]. Some of the first applications of QOC were in the interest of driving chemical reactions and studying nuclear magnetic resonance [23]. In these applications, lasers were controlled to create the pulse shape that caused the electronic transitions sought-after.

Some examples of QOC being woven into a control protocol can be found in [3, 21] where the goal was population transfer between the ground state ($|\psi_0\rangle$) and some goal state ($|\psi_g\rangle$) of the system. In [21], a Hamiltonian of the form

$\hat{H} = \hat{H}_0 + \lambda(t)\hat{H}_i$ was assumed where $\lambda(t)$ is the control function in the control problem. The goal was to find the control function that achieved the population transfer with as high probability as possible for a fixed total time for evolution, T. So, the "best" control function would drive the evolution to yield a final state $|\psi(T, \lambda)\rangle = |\psi_g\rangle$. The probability of the final state being the goal state is called the fidelity and is found by calculating $\mathcal{F} = \left|\langle\psi(T, \lambda)||\psi_g\rangle\right|^2$ which is also the population in the goal state. For this control problem, the cost function was the infidelity $(1 - \mathcal{F})$ and Krotov [13] numerical methods were used to find the control function that minimized it. The population transfer desired (labeled P_2 for "process 2") is achieved with high fidelity by implementing the control function shown in the top of Figure 1.1.
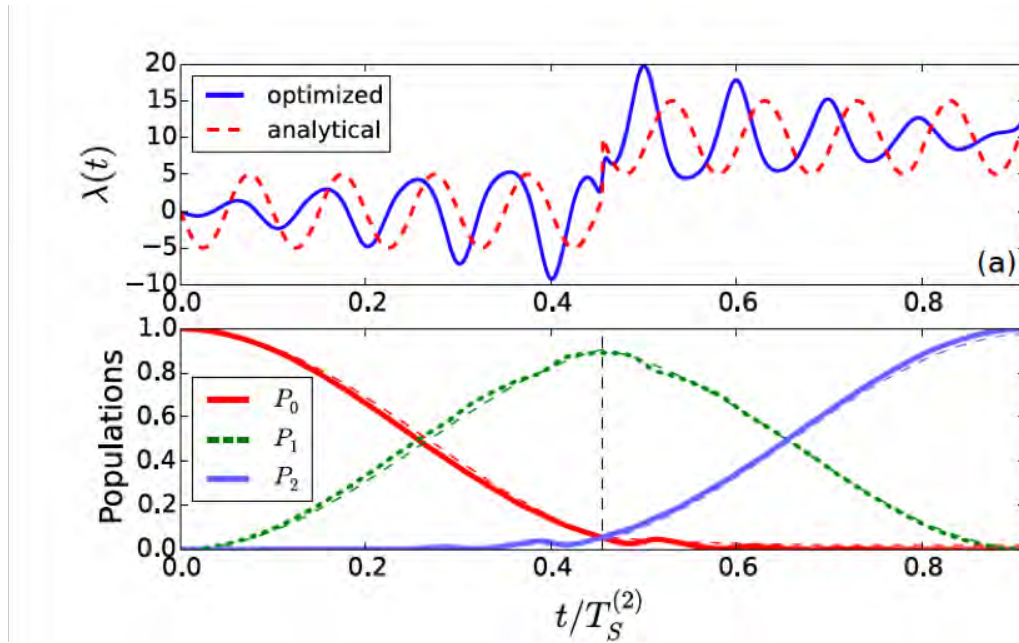
Figure 1.1: Top: Optimal control functions that achieve a process P_2 found with numerical and analytic methods are plotted. Bottom: The populations for several processes resulting from the control functions found are plotted. The main point here is that we see that the numerically determined optimal control function plotted in the top plot achieves total population transfer over the allotted time for process P_2 which proves that the control function does indeed minimize the infidelity. Reproduced from [21].

In the implementation of quantum logic gates for quantum computing, the procedure typically involves the maximization of the gate fidelity [18, 1]. Some of the most popular methods to optimize the cost function include GRAPE (gradient ascent pulse engineering) [12], the Krotov Algorithm [14, 13] and other gradient search algorithms. For our purposes, the method of choice will be a gradient-descent method using the Broyden – Fletcher – Goldfarb – Shanno (BFGS) algorithm to minimize the infidelity (probability of the final state not being equal to the final state) of state maps [10].

1.2 Controllability

In general, a control problem begins with a Hamiltonian of the following form:

$$\hat{H}(\vec{u}(t)) = \hat{H}_0 + \sum_{k=1}^{n} u_k(t)\hat{H}_k$$

H_0 is called the "drift" Hamiltonian and it is constant in time. The H_k are called the "control Hamiltonians" and are modulated in time by the functions $u_k(t)$. These functions are dependent on the classical fields that have parameters or settings that can be changed over time according to functions called the "control waveforms/functions." The goal is to determine the waveforms that achieve some dynamics, but first we must determine to which degree we can control the system.

There are many types of controllability ranging from completely controllable to pure state controllable. As the names imply, completely controllable means

that any possible unitary transformation on the Hilbert Space is achievable and pure state controllable means that any map from an arbitrary pure state to another is achievable. The controllability of a system can be determined by using properties of Lie Algebras and Lie Groups [7]. A Lie Group is a continuous group and the associated Lie Algebra is the tangent space at the identity of the Lie Group. Relevant examples of Lie Groups are $U(n)$ and $SU(n)$. $U(n)$ is the group of all $n \times n$ unitary matrices and $SU(n)$ is the group of all $n \times n$ unitary matrices with determinant 1, both with matrix multiplication as the operation on the groups. Their corresponding Lie Algebras are $u(n)$ and $su(n)$ with the commutator as the operation on the algebras.

For a given Hamiltonian, the dynamical Lie Algebra, $\mathcal{L}$, associated with the system is generated by $H_0, H_1, ..., H_n$. The dynamical Lie Algebra is always a sub-algebra of $u(n)$ where n is the dimension of the Hilbert Space. In particular, if the dimension of $\mathcal{L}$ is n^2 then it is exactly $u(n)$. If instead, the dimension is $n^2 - 1$, then $\mathcal{L} = su(n)$.

By the correspondence between Lie Groups and Lie Algebras, the Lie Group associated with the system is $e^{\mathcal{L}}$ and it is always a subgroup of $U(n)$. Furthermore, this Lie Group is the set of the reachable unitaries [7]. We see that if the Hilbert Space is of dimension n, then the set of all of unitary transformations is the Lie Group $U(n)$. Hence, for the system to be controllable the dynamical Lie Algebra would have to be $u(n)$ whose dimension is n^2. If the overall phase is irrelevant to the control problem, then for the system to be controllable it is sufficient for the dimension of the Lie Algebra to be $n^2 - 1$, $\mathcal{L} = su(n)$.

We determine the dynamical Lie Algebra by finding a basis that generates it. We can start the basis with operators from the Hamiltonian: $H_0, H_1, ..., H_n$. The

operation of the Lie Algebra is commutation so to create more basis elements, we take several commutators of different depths and repeat with the elements that are linearly independent (see Equations 1.1-1.3 for examples). This is done until no more linearly independent elements are generated or the dimension of the linearly independent set is n^2 or n^2-1, which implies complete controllability.

$$\text{Depth 1}: [\hat{H}_1, \hat{H}_1] := \hat{H}_1\hat{H}_2 - \hat{H}_2\hat{H}_1 \tag{1.1}$$

$$\text{Depth 2}: [\hat{H}_3, [\hat{H}_1, \hat{H}_1]] \tag{1.2}$$

$$\text{Depth 3}: [\hat{H}_4, [\hat{H}_3, [\hat{H}_1, \hat{H}_1]]] \tag{1.3}$$

1.3 Quantum Speed Limit

One of the biggest enemies of quantum control is state decoherence. The probability that decoherence occurs increases with time, so it is often in our best interest to do controls fast enough to avoid it. However, there exist fundamental, physical limitations that set bounds on how fast an evolution can occur successfully. This is called the Quantum Speed Limit (QSL) and there have been numerous analytical studies to determine bounds on the QSL. One of the first investigations on the QSL set bounds on evolution time for time-independent Hamiltonians that arise naturally from the energy-time uncertainty principle [16]. From this idea, there have been extensions to open quantum systems [8] where the QSL can be interpreted geometrically in the Hilbert space since it depends on the distance between the initial and final state ($\langle \psi_i | \psi_f \rangle$ where $|\psi_i\rangle$ is the

initial state and $|\psi_f\rangle$ is the final state). The time required also depends on the energy variance which speaks to the trade-off between time and energy required for an evolution:

$$t \geq \frac{\arccos(\langle\psi_i|\psi(t)\rangle)}{\overline{\Delta E}}$$

When analytic solutions are not possible we resort to numerical experiments to see what the QSL is for some desired evolution. Pareto front tracking can be used to see how the success of QOC depends on the time allotted for evolution [5].

CHAPTER 2

CONTROL OF A SPIN 1/2 SYSTEM ($SU(2)$)

We consider a spin-1/2 particle in a time-dependent magnetic field, $\vec{B}(t)$, that is a superposition of a field constant along the z-axis and a perturbative field oscillating along the x-axis with magnitude Ω, oscillation frequency ω, and phase ϕ. The constant field produces Zeeman splitting and has eigenstates $|\uparrow\rangle, |\downarrow\rangle$ called "spin-up" and "spin-down" respectively. These are the standard basis states for two-dimensional Hilbert Space. Our goal is to achieve an evolution from spin-down to an arbitrary target state. The perturbative field, also called the driving field, is essential to the control problem since the unperturbed field itself would not be enough to achieve an arbitrary target state. It is also called the driving field because it drives spin magnetic resonance. That is, given the right parameters, when the system is driven at resonance ($\omega = \omega_0$) the probability of being one of the standard basis states oscillates.

Our Hamiltonian is taken to be of the following form:

$$\hat{H}(t) = -\hat{\vec{\mu}} \cdot \vec{B}(t) = \frac{\hbar\omega_0}{2}\hat{\sigma}_z + \frac{\hbar\Omega}{2}\cos(\omega t + \phi)\hat{\sigma}_x$$

Now, we review the dynamics of spin resonance dynamics which is at the heart of this control protocol [9]. We begin by transforming to the rotating frame at the magnetic field frequency, ω, by using the unitary operator $\hat{U}_{RF} = e^{-i\frac{\omega t}{2}\hat{\sigma}_z}$. A state $|\psi\rangle$ is mapped to the rotating frame by $|\psi(t)\rangle_{RF} = \hat{U}_{RF}^\dagger |\psi(t)\rangle$. Using this and the Schrödinger Equation, we find the Hamiltonian in the rotating frame (Eq. 2.1 - Eq. 2.4). The Hamiltonian in the rotating frame, $\hat{H}_{RF}$, is made up of two terms. One is what we call the effectively rotated Hamiltonian because it is a

similarity transformation of the original. The other term is a fictitious magnetic field propagating in the negative z-direction with magnitude ω resulting from changing to a rotating frame.

$$i\hbar \frac{\partial |\psi(t)\rangle_{RF}}{\partial t} = i\hbar \frac{\partial \hat{U}_{RF}^\dagger |\psi(t)\rangle}{\partial t} \tag{2.1}$$

$$= i\hbar \left(\hat{U}_{RF}^\dagger \frac{\partial |\psi(t)\rangle}{\partial t} + \frac{\partial \hat{U}_{RF}^\dagger}{\partial t} |\psi(t)\rangle \right) \tag{2.2}$$

$$= \left(\hat{U}_{RF}^\dagger \hat{H} \hat{U}_{RF} - \frac{\hbar\omega\hat{\sigma}_z}{2} \right) |\psi(t)\rangle_{RF} \tag{2.3}$$

$$= \hat{H}_{RF} |\psi(t)\rangle_{RF} \tag{2.4}$$

We obtain an explicit expression for the Hamiltonian in the rotating frame (see Equations 2.5-2.7). $\hat{\sigma}_+, \hat{\sigma}_-$ are the raising and lowering operators. Examining the expression, we discover two important pieces of information. Firstly, we note that the strength of what was the strong field (ω_0) is now the detuning, $\Delta := \omega - \omega_0$ which quantifies how far the magnetic field frequency is from the spin resonance frequency. On resonance, this term vanishes. Another important note is that we can interpret the driving field as being composed of co-rotating and counter-rotating fields such that when we went into the rotating frame, one of them became a time-independent field and another that is oscillating with frequency 2ω.

$$\hat{H}(t) = \frac{\hbar\omega_0}{2}\hat{\sigma}_z + \frac{\hbar\Omega}{4}(e^{i\omega t}e^{i\phi} + e^{-i\omega t}e^{i\phi})(\hat{\sigma}_+ + \hat{\sigma}_-) \tag{2.5}$$

$$\implies \hat{H}_{RF}(t) = \frac{\hbar\omega_0}{2}\hat{\sigma}_z + \frac{\hbar\Omega}{4}(e^{i\omega t}e^{i\phi} + e^{-i\omega t}e^{i\phi})(\hat{\sigma}_+e^{i\omega t} + \hat{\sigma}_-e^{-i\omega t}) - \frac{\hbar\omega\hat{\sigma}_z}{2} \tag{2.6}$$

$$= -\frac{\hbar\Delta}{2}\hat{\sigma}_z + \frac{\hbar\Omega}{4}((\hat{\sigma}_+e^{2i\omega t}e^{i\phi} + \hat{\sigma}_-e^{-2i\omega t}e^{-i\phi}) + (e^{-i\phi}\hat{\sigma}_+ + e^{i\phi}\hat{\sigma}_-)) \tag{2.7}$$

Now we apply the RWA to obtain:

$$\hat{H}_{RF}(t) \approx -\frac{\hbar\Delta}{2}\hat{\sigma}_z + \frac{\hbar\Omega}{2}\left(\cos\phi\hat{\sigma}_x + \sin\phi\hat{\sigma}_y\right) \tag{2.8}$$

Therefore, if $\Omega \ll \omega$ and $\Delta \ll \omega_0$, then the terms with $e^{\pm 2i\omega t}$ are oscillating much faster than the rest of the frequencies that dictate the dynamics. This would permit the application of the rotating wave approximation (RWA) which averages the fast-oscillating terms to zero because they have no significant effect on the dynamics. If we write the state as $|\psi\rangle = c_\uparrow |\uparrow\rangle + c_\downarrow |\downarrow\rangle$, then the Schrödinger equation would yield differential equations for the coefficients of the coherent superposition (see Equations 2.9-2.10). On resonance, the solutions are Rabi oscillations with period $\frac{2\pi}{\Omega}$. The shortest amount of time needed to transfer the state from spin-down to spin-up is $\frac{\pi}{\Omega}$.

$$\dot{c}_\uparrow = -\frac{i}{2}\left(\Delta c_\uparrow + \Omega e^{-i\phi}c_\downarrow\right) \tag{2.9}$$

$$\dot{c}_\downarrow = -\frac{i}{2}\left(\Omega e^{i\phi}c_\uparrow - \Delta c_\downarrow\right) \tag{2.10}$$

When the parameters do not satisfy these conditions, the RWA is not valid and the dynamics are not so straightforward. However, these conditions are

typically satisfied and the RWA becomes a very good approximation. For example, in the case of the Cesium-133 clock transition, we have $\omega_0/2\pi \approx 9.19\text{GHz}$, $\Delta/2\pi, \Omega/2\pi \sim 10\text{kHz}$. For this reason we assume for the remainder of this chapter that we are driving at resonance and $\Omega << \omega$ and adopt the Hamiltonian from Eq. 2.8 for our control problem.

2.1 SU(2) Controllability

So far, we have been treating ϕ as a time-independent parameter but this would affect the extent of our controllability. If the phase is constant, then the Hamiltonian is time independent and the time evolution operator is simply $\hat{U} = e^{-i\frac{\hat{H}t}{\hbar}}$. One special property of $SU(2)$ is that it is closely related the group of 3×3 rotation matrices, $SO(3)$ [22]. In fact, all unitaries can be written in the form $\exp\left\{-i\frac{\theta}{2}\hat{\vec{\sigma}} \cdot \vec{e}_n\right\}$ which is the quantum mechanical operator for a rotation of a spin-1/2 particle of angle θ about the real unit vector $\vec{e}_n$. In particular, these operators can describe the rotation from some initial state $|\psi_i\rangle$ to a final state $|\psi_f\rangle$ which can be plotted as vectors on the Bloch sphere (Figure 2.1).

Suppose we drive the system at resonance, then the time evolution operator is a rotation of angle Ωt about a unit vector on the x-y plane defined by azimuthal angle ϕ (Eq. 2.11). This means that if the phase is constant then we would only be allowed to do rotations about a single axis defined by ϕ. To make our control more flexible, we make the phase time-dependent ($\phi \rightarrow \phi(t)$) that we can tailor as we need.
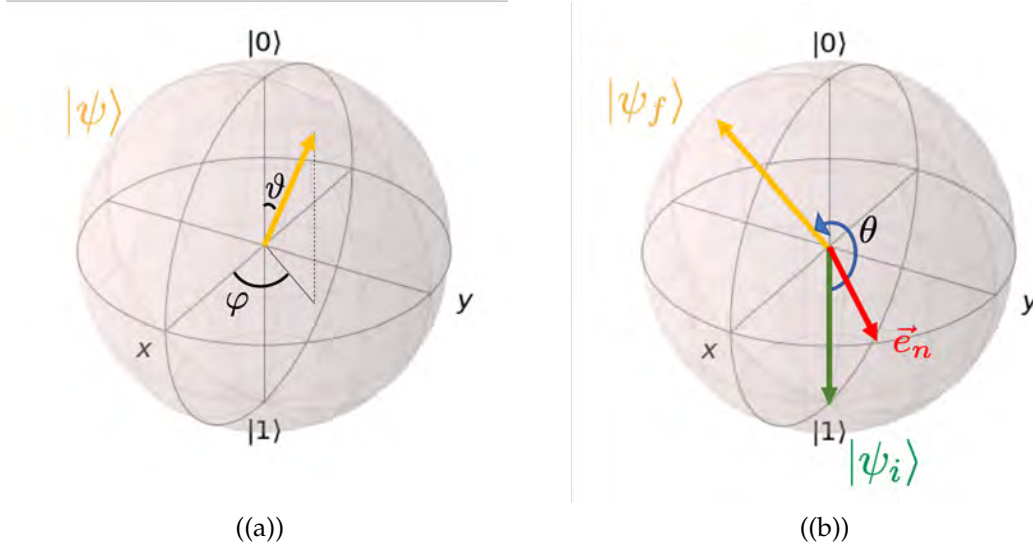
Figure 2.1: a) Any pure state, $|\psi\rangle$, can be represented by a unit vector defined by angles φ, ϑ which define the state as a superposition of spin-up and spin-down (Eq. 2.16). b) A rotation of angle θ about the unit vector $\vec{e}_n$ takes the initial state $|\psi_i\rangle$ to the final state $|\psi_f\rangle$. This rotation can be represented by the unitary transformation in Equation 2.11.

$$\exp\left(-i\hat{H}(\phi)t/\hbar\right) = \exp\left(-i\frac{\Omega t}{2}\hat{\vec{\sigma}} \cdot (\cos(\phi)\vec{e}_x + \sin(\phi)\vec{e}_y)\right) \tag{2.11}$$

The dimension of the Hilbert space is $d = 2$, so the Lie Group of all unitaries acting on the Hilbert Space is *SU(2)* (neglecting overall phases). A basis for the corresponding Lie Algebra, *su(2)*, is known to be the set of Pauli matrices (Eq. A.1). So in order to have a controllable system, we would want the dynamical Lie Algebra to generate all of the Pauli matrices. For the control we will consider the Hamiltonian to be at resonance, leaving $\hat{\sigma}_z$ out of the Hamiltonian. Thus, we have to prove controllability with the remainder of the Hamiltonian which means that the basis elements that we start with are $\hat{\sigma}_x, \hat{\sigma}_y$. According to the process outlined for showing complete controllability, the next step is to take the commutator $[\hat{\sigma}_x, \hat{\sigma}_x]$. The result is a term proportional to $\hat{\sigma}_z$ so we have

obtained all of the generators of the Lie Algebra *su*(2) once more and the system is controllable.

2.2 Optimal Control of SU(2)

The infidelity is a measure of how much overlap there is between the final state of an evolution and some target state (Eq. 2.12), and for this optimal control problem, it will be the cost function we minimize over the control function, $\mathcal{I}(\phi)$. When the final state is exactly the target state, the infidelity is zero. Thus, we want to find the control function that will make achieve an infidelity less than some defined tolerance. We restrict our search for the optimal control function to piecewise constant functions defined by N equal number of pulses over a total time T (Eq. 2.13).

$$\mathcal{I}(\phi) = 1 - \mathcal{F}(\phi) = 1 - |\langle \psi_{targ}| \hat{U}(\phi) |\psi_0\rangle|^2 \tag{2.12}$$

$$\phi(t) = \begin{cases} \phi_0 & 0 \le t < \frac{T}{N} \\ \phi_1 & \frac{T}{N} \le t < 2\frac{T}{N} \\ \vdots \\ \phi_{N-1} & (N-1)\frac{T}{N} \le t < N\frac{T}{N} = T \end{cases} \tag{2.13}$$

This choice for the control function also makes the Hamiltonian piecewise constant. The solution to the Schrödinger equation for the time evolution op-

erator when the Hamiltonian is constant is $e^{-i\frac{\hat{H}(\phi)_n \delta t}{\hbar}}$ so the total time evolution operator from $t = 0$ to the total time T is the product of unitaries for each constant Hamiltonian (Equation 2.14). Further, note from Equation 2.15 that the total unitary transformation is the product of rotations of angle $\Omega \delta t$ about the unit vector $\cos(\phi_n)\vec{e}_x + \sin(\phi_n)\vec{e}_y$.

$$\hat{U}(\phi) = e^{-i\hat{H}(\phi_{N-1})\delta t/\hbar} \cdots e^{-i\hat{H}(\phi_0)\delta t/\hbar} \tag{2.14}$$

where

$$e^{-i\hat{H}(\phi_n)\delta t/\hbar} = \exp\left(-i\frac{\Omega \delta t}{2}\hat{\vec{\sigma}} \cdot (\cos(\phi_n)\vec{e}_x + \sin(\phi_n)\vec{e}_y)\right) \tag{2.15}$$

The number of pulses (N) and the total time of the evolution (T) will affect which control function is found. We seek to study the relationship between these quantities in order to gain information about the trade-off between resources. From the point of view of controllability, we know that if we were able to implement a control function with infinite bandwidth over a time greater than the QSL, then we would certainly minimize the infidelity. However, we do not have such resources available so we will search for the control function that can be applied near the quantum speed limit and see what sort of bandwidth is required.

2.3   Algorithm for Optimal Control

We optimize the infidelity with respect to $\phi(t)$ using the Broyden – Fletcher – Goldfarb – Shanno (BFGS) algorithm [10]. BFGS is an iterative algorithm that

searches for stationary points of a cost function. The general idea is that starting at some random ϕ, the algorithm calculates the gradient at nearby points and follows the paths with negative gradient until it is sufficiently close to zero. Note that since the control function is piecewise constant, the control landscape isn't smooth but it is smooth enough to converge if such a stationary point exists[15]. "Sufficiently close" is chosen to be an infidelity 10^{-8}. This can be understood because the angle between the final and target states can be found with the inner product $\langle \psi_{targ} | \psi_f \rangle = \cos \theta$. If $\theta = 10^{-4}$, the states are very close to being the same. Thus, the infidelity in the small-angle approximation would be 10^{-8}:

$$\mathcal{I} = 1 - \cos^2 \theta = \sin^2 \theta \approx \theta^2$$

To study the quantum speed limit of the system we use the idea of Pareto efficiency which began in the context of economics. Oftentimes, we have resources that we want to optimize but can not be modified independently of others. So, Pareto efficiency is reached when we can have all resources as close to optimal as we can. This state of being "Pareto efficient" can be searched for using Pareto front tracking. By producing a curve that demonstrates the trade-off between some resources we can find the most optimal point [5]. A demonstration is shown in Figure 2.2.

In our case, we want to find the smallest time for which we can find a control waveform that optimizes the infidelity. We search for the Pareto front by fixing the number of pulses, initial and target state, and Rabi frequency. Then, we use BFGS to find an optimal control waveform for several total times T allotted to do the control. These total times are distributed from zero to a time well past
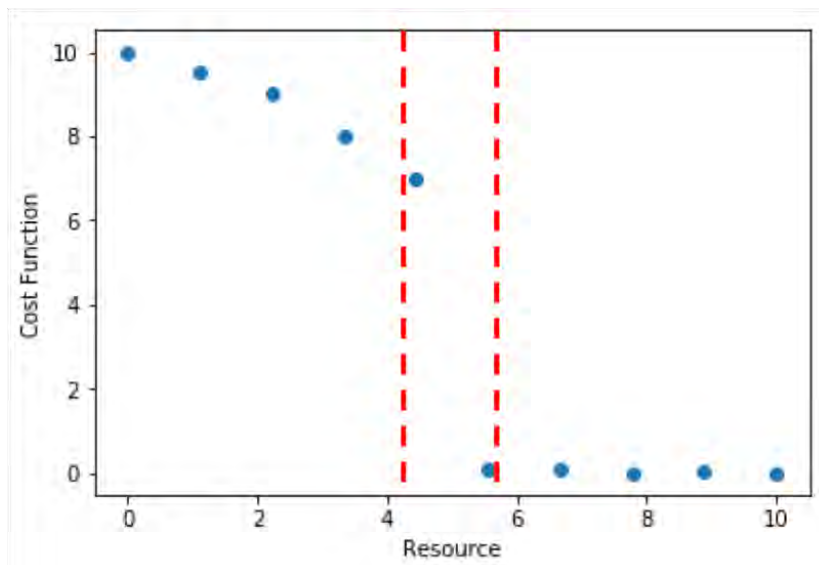
Figure 2.2: This is a representation of what a plot might look like when looking for the Pareto front. By plotting the value of the cost function we want to minimize versus some resource that we also want to minimize we can find the optimal resource value. In this case, we can clearly see that when the resource is in the region from 4-6, the cost function can't be minimized successfully. Thus the Pareto front is in this region.

the QSL. With this data, we produce a plot of optimal infidelity versus total control time (plots are shown in Section 2.4). This is repeated for many random target states and then the average of the optimal infidelities is calculated for each total time. From these results, the Pareto front from is identified as the region containing the smallest time where the infidelity was optimized below the threshold (Section 2.4).

To sample random states uniformly from the Hilbert Space, we think about its topology. Since it is $SU(2)$ is closely related to $SO(3)$, then each state can be mapped to a point on the surface of the Bloch sphere. Any pure state can be thought of as a unit vector, $\vec{e}_n$, on the Bloch sphere defined by the azimuthal(φ) and the polar (ϑ) angles.

$$|\uparrow\rangle_n = \cos(\vartheta/2)\,|\uparrow\rangle + e^{i\varphi}\sin(\vartheta/2)\,|\downarrow\rangle \tag{2.16}$$

A differential element of area on the sphere does not depend uniformly on the polar angle, ϑ, as the dependence is $\sin\vartheta$. Instead it follows a sinusoidal distribution (Eq. 2.17) since there is more probability of a point being at the equator than at the poles. From Eq. 2.17 we see that the quantity $\cos(\vartheta)$ is uniformly distributed on the sphere so to get a uniformly distributed azimuthal angles we can make a change of variables $-\cos\vartheta \rightarrow \xi$ which has a range of $[-1, 1]$. We can then sample random ξ with built-in functions in and then take the inverse cosine of it to obtain a random ϑ.

$$dA = \sin(\vartheta)d\varphi d\vartheta = d\varphi d(-\cos(\vartheta)) \tag{2.17}$$

From our knowledge of the dynamics of the system, we know that an important time scale is $\frac{\pi}{\Omega}$ since it is the minimum amount of time required to transfer spin-down to spin-up. Thus, we would expect for the QSL to be less than or equal to this time and a reasonable maximum total time for Pareto front tracking is $4\frac{\pi}{\Omega}$. One of the parameters that needs to be fixed for the algorithm is the number of pulses. Since we are interested in the relationship of total time and number of pulses, then we would like to use various values of N. What are some reasonable values of N? The number of pulses refers to the number of rotations that are done to go from spin-down to the target state so we can think of how many parameters are needed to find the right rotation. The target state is defined by two parameters since there are $2 * D = 4$ real parameters but there are

18

two restrictions, normalization and neglecting overall phase. Thus, a reasonable set of number of pulses to fix are $N \in 2, 3, 4, 5, 6$.

2.4   SU(2) Results

The results shown in Figures 2.4(a)-2.4(e) are the average of 20 random target states. The QSL is close to $\frac{\pi}{\Omega}$ on average. It is evident from the plots for $N = 2, 3, 4$ that there is oscillatory behavior of the optimized fidelity. This can be understood by thinking about the dynamics on the Bloch sphere. Suppose we wanted to evolve the system from spin-down to spin-up. If $N = 1$ we can rotate about any axis, $\vec{e}_n$, so ϕ could take any value but we would require a total time of the form $(2k + 1)\frac{\pi}{\Omega}$, $k \in \mathbb{N}$ to achieve a pi-pulse (Figure 2.3). If the total time was an even multiple of $\frac{\pi}{\Omega}$, then we would be doing 360 degree rotations which would yield spin-down as the final state.

By understanding this behavior, we see when N is small we don't have the freedom to do all rotation necessary meaning that we have to pick our rotations carefully. As we have larger N we have access to more rotations so we can achieve target states more easily and the infidelity curve becomes flatter. This trend is seen as N increases in Figures 2.4(a)-2.4(e). From indicate that if one wants to ensure that an optimal control waveform is found for an arbitrary state map, a good idea would be to increase N and let the system evolve for a time greater than the QSL.

A particularly interesting result from Figure 2.4(a) is that with two pulses, every state could be achieved even at the QSL. This suggests that given any random target state, there exist two rotations that will take spin-down to the
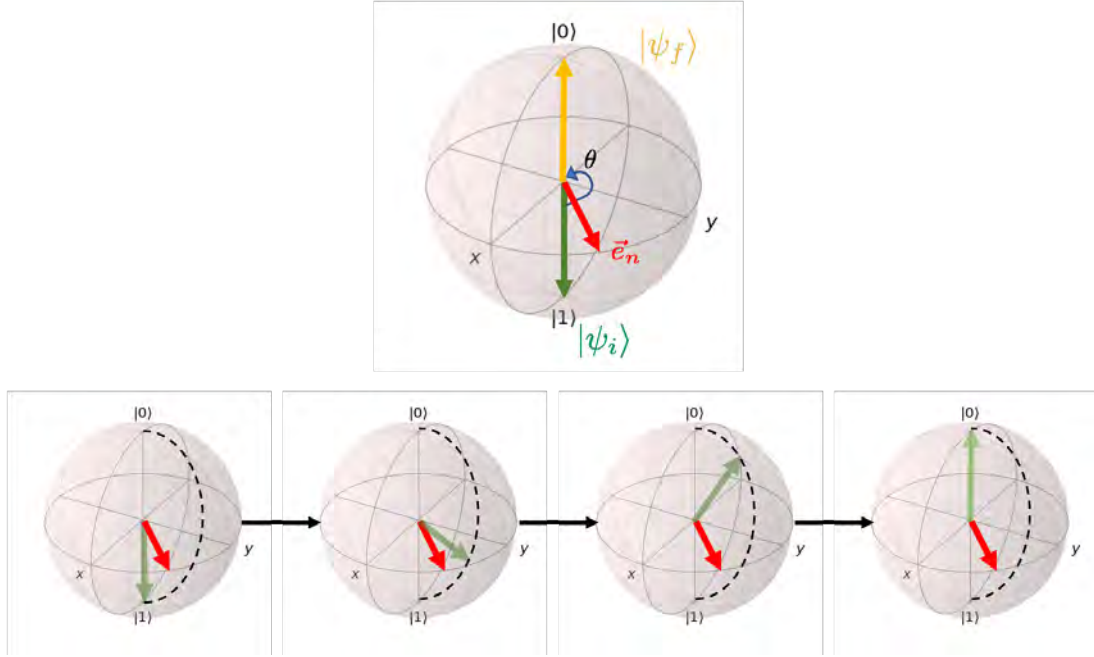
Figure 2.3: The Bloch sphere at the top shows the initial state (green), target state (yellow-orange), torque vector about which to rotate (red), and the angle of rotation θ. To successfully rotate spin-down to spin-up, θ must be an odd multiple of π. According to Equation 2.15, the angle of rotation is $\Omega\delta t$. Thus, to achieve this desired state map, we must apply a pulse for $\Omega\delta t = \pi$. That is for a time $\delta t = \frac{\pi}{\Omega}$.

target state with optimal infidelity. These two rotations are of the same angle but about two different axes on the x-y plane. This happens when the allotted control time is of the form $(2k + 1)\frac{\pi}{\Omega}$, $k \in \mathbb{N}$. Because the sphere is isotropic this can be generalized to the following statement.

Conjecture 2.4.1 *Given any two unit vectors on the Bloch sphere, there exists a sequence of two rotations that will take one vector to the other. In particular these rotations are by the same angle about axes on a plane perpendicular to one of the given vectors.*
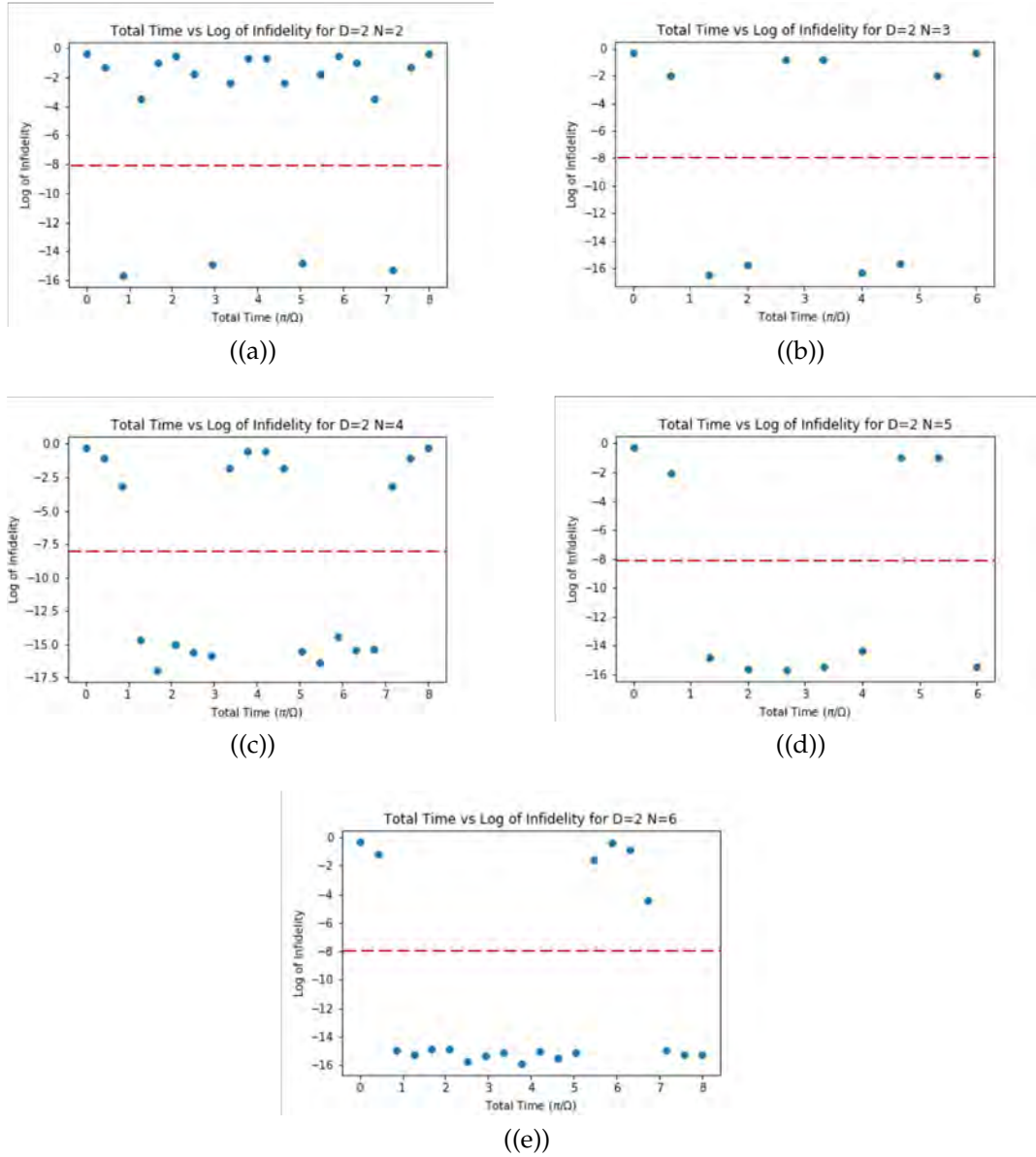
Figure 2.4: The optimal infidelity achieved for 20 target states for different total times is averaged for a control waveform with (a) 2 pulses, (b) 3 pulses, (c) 4 pulses, (d) 5 pulses, and (e) 6 pulses. On the y-axis is the log of the averaged infidelity and the x-axis is of the total times in units of π/Ω. The threshold is marked by the dashed red line at -8.
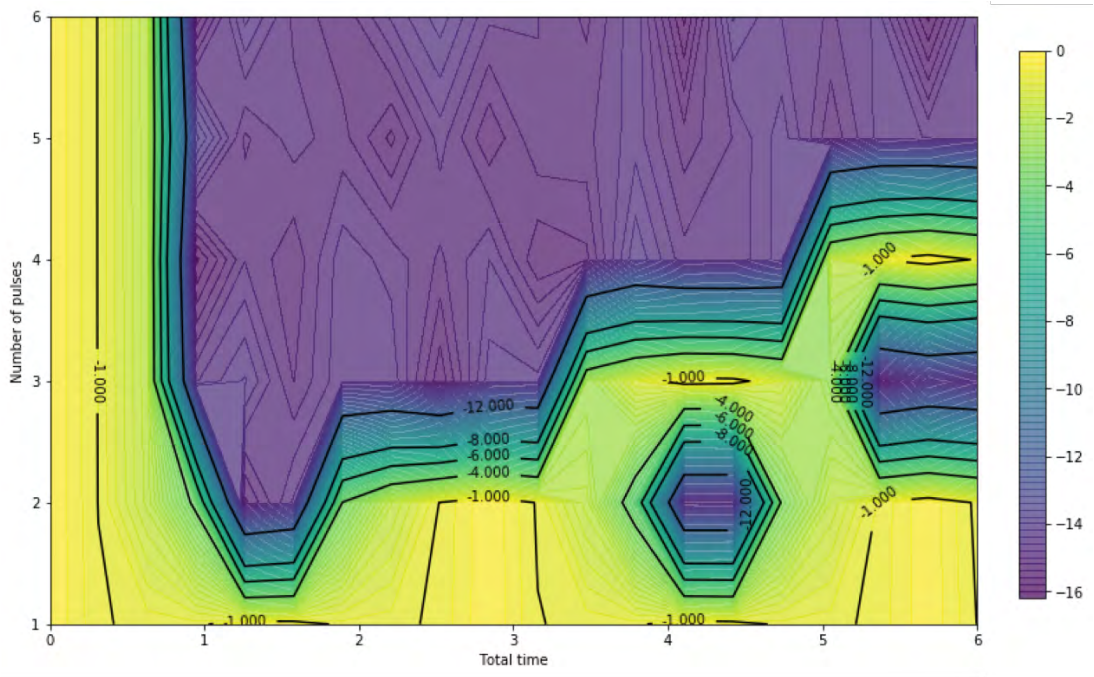
Figure 2.5: Contour plot of the average infidelity over 20 random target states at different (T, N) points for optimal control of spin-1/2.

CHAPTER 3

CONTROL OF SPIN J

We now consider the system of a particle with spin greater than $1/2$ in the presence of electromagnetic fields. The controllability of a Hamiltonian for this system can not be determined as trivially as in the case for spin-$1/2$ because the dimension of the Lie Algebra is required to be larger than the size of the set of angular momentum operators. What this means is that it is not enough for the Hamiltonian to include $\hat{J}_x, \hat{J}_y, \hat{J}_z$ (Eq. A.4). In addition, the dynamics for these systems can not be mapped to a space that we can visualize so they are not as predictable as with spin-$1/2$. However, we can still design a controllable Hamiltonian and solve for the dynamics. QOC is implemented in the same way as with the spin-$1/2$ case and the QSL is searched for in the same way as well. What changes are the ranges for the total time and number of pulses that we use to define the control waveform. The controllability of the Hamiltonian and the observed trade-off between the control resources are discussed.

3.1 Controllability

We recall that for a system of a particle with spin j, the dimension of the Hilbert Space is $d = 2j + 1$. This is understood because the standard basis states are the eigenstates of the angular momentum operator along the z-axis, $\hat{J}_z$. These eigenstates are denoted $|m\rangle$ for $m \in \{-j, -j + 1, ..., j - 1, j\}$. The unitary operators acting on this Hilbert space, neglecting overall phases, make up the Lie Group $SU(d)$. This means that the generating set is of size $d^2 - 1$.

Suppose we want to control a spin-1 particle. The Hilbert space is of dimension 3 so the generating set of the Lie Algebra *su*(3) contains 8 elements. Clearly, if the Hamiltonian was of the same form like in the case of the spin-1/2, then it would not be controllable because the commutator of the angular momentum operators is $[\hat{J}_i, \hat{J}_j] = i\hbar\epsilon_{ijk}\hat{J}_z$ and do not generate enough basis elements, it only produces 3 $(\hat{J}_x, \hat{J}_y, \hat{J}_z)$. Even if we took commutators of elements in this set, no new operators would be generated and we would never obtain a set of linearly independent elements that span a space with dimension 8. This is true for any higher spins $j \geq 1$. As a result, it is necessary to include another generating term in the Hamiltonian. It turns out that it is sufficient to include a term proportional to $\hat{J}_z^2$ [17]. For the case of spin-1/2, $\hat{J}_z^2$ is the identity operator so it wouldn't add any more terms to the generating set. Thus, we will use the following completely controllable Hamiltonian to control our state maps in *d*-dimensional ($d \geq 3$) Hilbert Space.

$$\hat{H}(\phi(t)) = \hbar\Omega(\cos(\phi(t))\hat{J}_x + \sin(\phi(t))\hat{J}_y) + \hbar\kappa\hat{J}_z^2$$

3.2   Optimal Control of SU(d)

The dynamics of a larger spin and the topology of *SU(d)* ($d > 2$) are more of a mystery to us than those of *SU(2)*. We are not able to visualize the dynamics similar to the way we did before. However, because of the intuition that we gained in Chapter 2 we are able to make some educated decisions on parameter choices. For example, the range of number of pulses, *N*, that we looked at

were from $2d$ to $2d + 4$ and the total time up to $(4d)\frac{\pi}{\Omega}$. We also choose $\Omega = \kappa$. By choosing them to be equal, we have the two components of the Hamiltonian acting equally instead of one being a perturbation. This choice, however, could be changed and it would affect the dynamics which could be something interesting to look into further in future research.

Since we want to average the results over many random states and thus get a more complete picture of resource trade-off we must have a way of sampling random target states uniformly. We got a sneak peak of how we must be careful with how we pick random states from $SU(2)$ to ensure a uniform distribution. Rrandom states in d-dimensional Hilbert Space can be producds by applying a random unitary matrix on a fiducial state. These random unitary matrices are elements of the group $G = U(d)$ which is a locally compact topological group. Groups like these have an associated Haar measure, μ [19].

Definition 3.2.1 (Haar Measure) *The Haar Measure, μ, on a locally compact topological group G is one that satisfies the following condition for all $g \in S \subseteq G$.*

$$\mu(gS) = \mu(Sg) = \mu(S) := \int_{g \in S} d\mu(g)$$

A *measure* defined on a set is used to measure the "size" of a subset. Furthermore, if $\mu(G) = 1$, then μ is a probability measure on G. We can take advantage of this by finding a probability density function $f(g)$ on G which in turn becomes a probability distribution from which we can sample random elements of the group. The appropriate function for the general group $U(d)$ was found in [24] and it was shown that the right distribution is produced by orthogonalizing any random matrix, $Z \in \mathbb{C}^{dxd}$, using the Gram-Schmidt process [19, 11].

Thus, to create a random state, we generate a random unitary matrix and

then multiply this with a unit vector from the Hilbert Space. For our purposes, our fiducial state vector was of the form (0,0,...,0,1).

3.3 Results

The results shown here are for Hilbert Space dimensions of 3, 4, and 5. The plots are grouped by dimension and are differentiated by the number of pulses that the control waveform was defined by. We observe what the QSL is for each of the dimensions and also the minimum number of pulses required to optimize the infidelity.

The QSL for spin-1 ($d = 3$) seems to be between $\frac{\pi}{\Omega}$ and $2\frac{\pi}{\Omega}$. The smallest number of pulses required to have optimal infidelities reached is $N = 5$. There is some oscillatory behavior in the infidelity similar to that seen for $SU(2)$. As the number of pulses increases, we see that the curve flattens out as well.

The QSL for $d = 4$ seems to be $2\frac{\pi}{\Omega}$. The smallest number of pulses required to achieve optimal infidelities is $N = 7$.

The QSL for $d = 5$ seems to be between $3\frac{\pi}{\Omega}$ and $4\frac{\pi}{\Omega}$. The smallest number of pulses required to achieve optimal infidelities is $N = 10$.

We observe that with higher bandwidth (more N) one can ensure that a desired state map can be achieved with high fidelity even for times near the QSL. This is what would be expected but something that is interesting is how the optimal infidelity behaves for small N. In the case of the spin-1/2, we understand the oscillatory behavior because of the topology of the Hilbert Space so it is most likely the case that the behavior we see for higher dimensions is also a result of

26
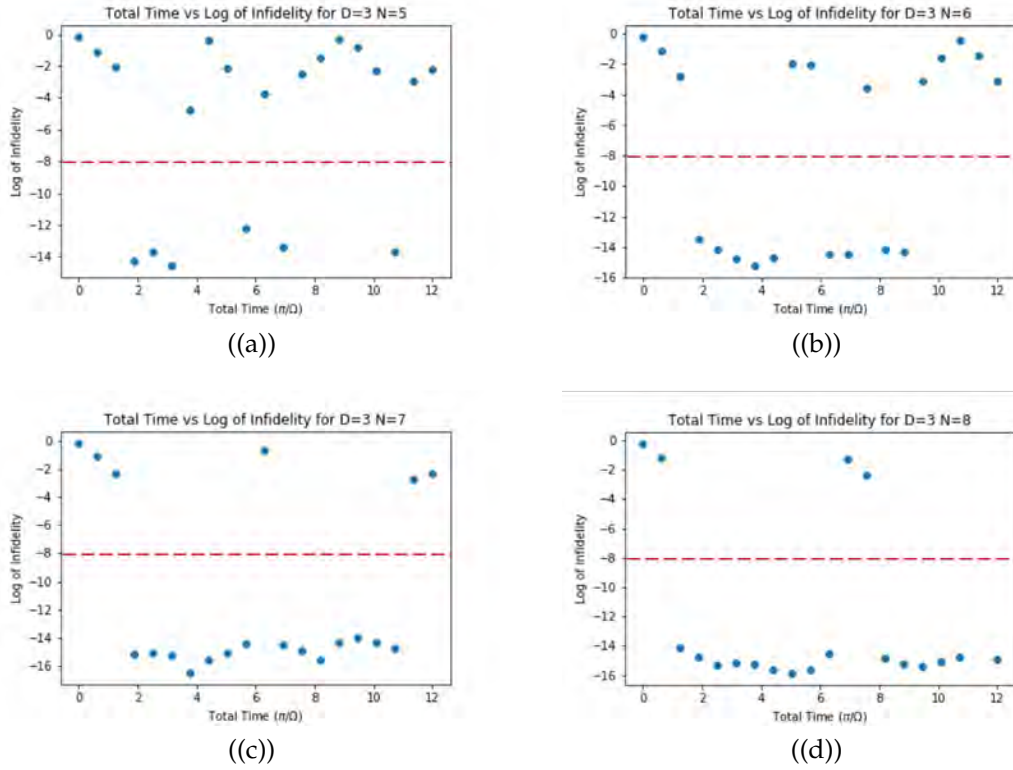
Figure 3.1: We considered the system for spin 1, $d = 3$. Plots show average optimal infidelities versus total control time achieved for (a) 5, (b) 6, (c) 7, and (d) 8 pulses. The average was taken over 20 random target states and threshold is marked by dashed red line at -8.

the topology of higher dimensional Hilbert Space.

Table 3.1: Summary of Results per Dimension

d	N_{min}	$QSL(\frac{\pi}{\Omega})$
2	2	0.5-1
3	5	1-2
4	7	2-3
5	10	3-4

Table 3.2: Summary of minimum number of pulses, N_{min}, and range of the QSL required for the state maps to be achieved with optimal fidelity for dimensions seen in Figures 2.4 - 3.4.

27
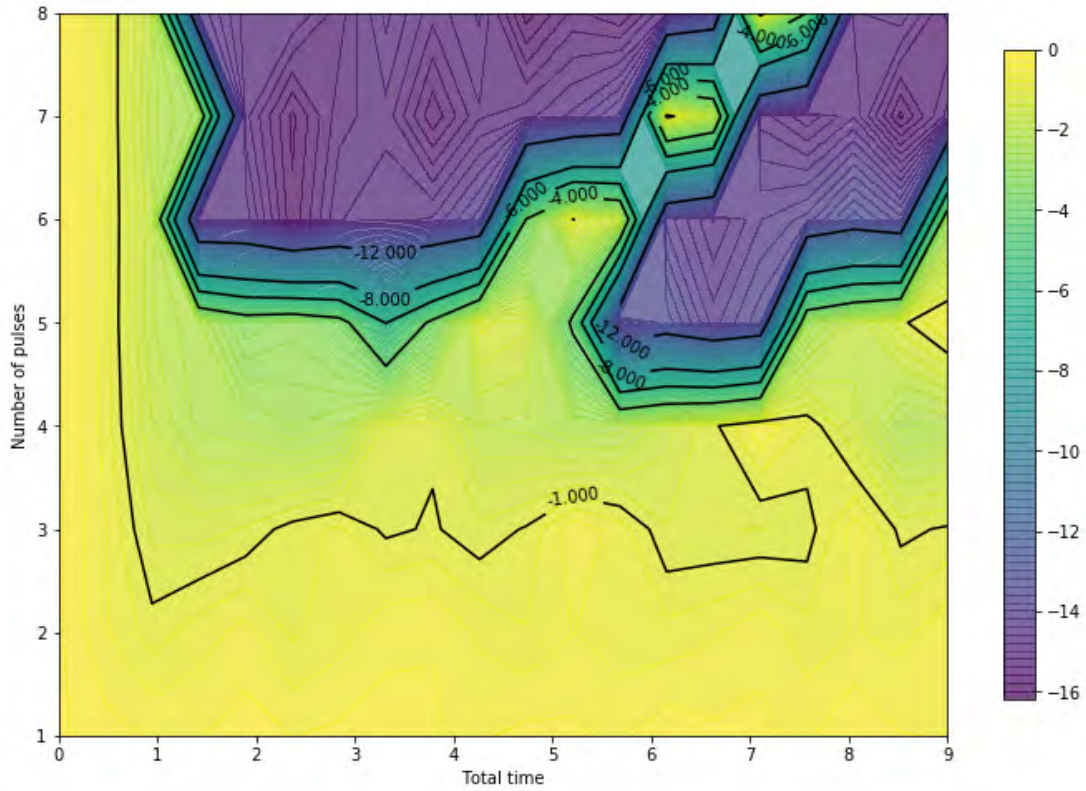
Figure 3.2: Contour plot of the average infidelity over 20 random target states at different (T, N) points for optimal control of spin-1.

((a))

((b))
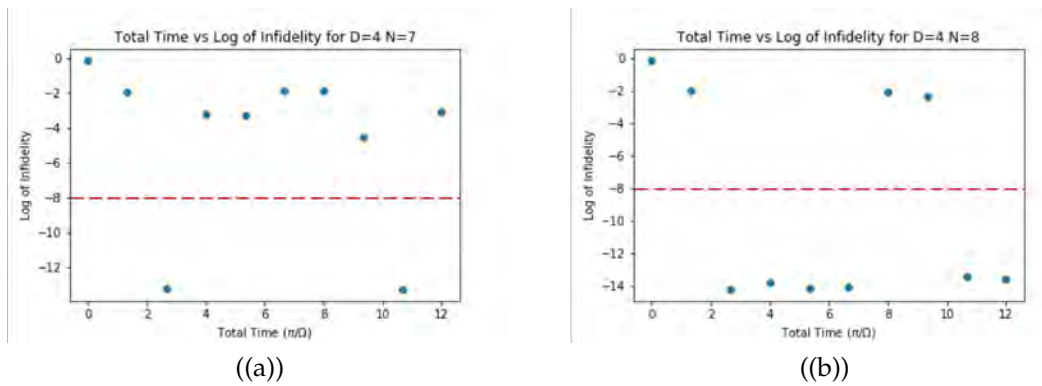
Figure 3.3: We considered the system for spin $3/2$, $d = 4$. Plots show average optimal infidelities versus total control time achieved for (a) 7 and (b) 8 pulses.The average was taken over 20 random target states and threshold is marked by dashed red line at -8.
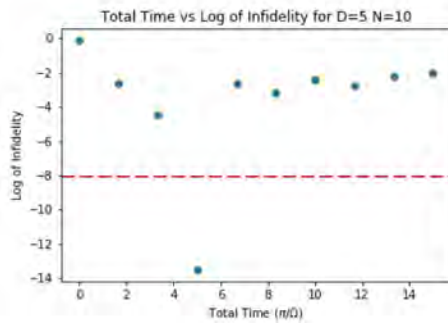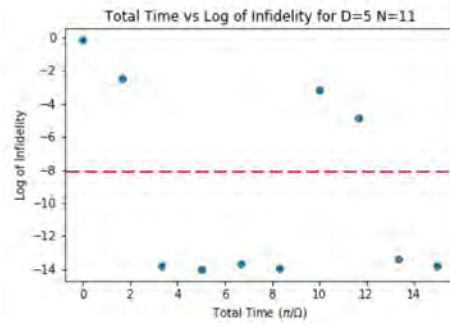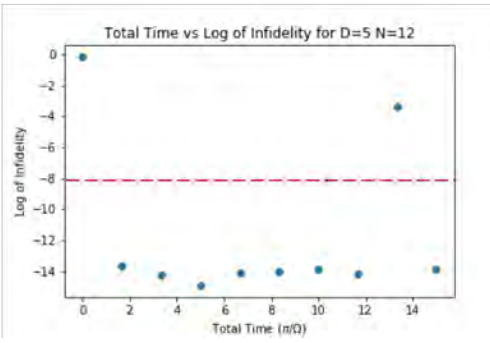
Figure 3.4: We considered the system for spin 2, $d = 5$. Plots show average optimal infidelities versus total control time achieved for (a) 10, (b) 11 and (c) 12 pulses.The average was taken over 20 random target states and threshold is marked by dashed red line at -8.

CHAPTER 4

CONCLUSION AND OUTLOOK

In this thesis, we investigated the relationship between time and bandwidth needed to successfully implement optimal quantum control for closed systems of spins. We began with the system of a spin-1/2 particle in the presence of a magnetic field with a component constant component along the z-axis and a driving component oscillating along the x-axis. By transforming to the rotating frame, spin resonance dynamics are produced by choosing the detuning, Δ and the Rabi frequency, Ω, to be much smaller than the driving frequency, ω, and thus be allowed to make the RWA. This helped us gain intuition on how a control protocol could be designed and we obtained a controllable Hamiltonian [9]. The controllability of the Hamiltonian is shown by demonstrating that the operators in the Hamiltonian generate the Lie Algebra $su(2)$ which in turn means that any unitary in $SU(2)$ can be reached.

The phase shift, ϕ, of the transverse field is chosen as the control waveform and because of the relationship between $SU(2)$ and $SO(3)$ [22], we can interpret ϕ as the azimuthal angle of the axis on the x-y plane about which the spin rotates. Thus, by choosing the control waveform, $\phi(t)$, to be a piecewise constant function, the goal of the optimal control algorithm is to find the sequence of rotations that achieves the desirable state map and minimizes the infidelity. The control waveform is defined by T, the total time of the evolution and N, the total number of pulses. The pulses are each applied for a time T/N. T, N and the optimal infidelity achieved by the optimal control algorithm are related in a complex way that give us information on the time and bandwidth needed for a control. We can observe how the optimal infidelity changes with the total time

of the evolution by plotting the optimal infidelity achieved versus total time of evolution for a given desirable state map. For simplicity our state maps were from spin-down to a random state sampled uniformly from the surface of the Bloch sphere. The Pareto front seen on the plot, which is where the infidelity can not be optimized, indicates the QSL time [5].

To get a general view of the QSL, this data was gathered for several random target states for a specified number of pulses, N, and the average of the optimal infidelity was taken at each total time. Several plots were created with this data for various N. The data demonstrated that the QSL approached $\frac{\pi}{\Omega}$. This is reasonable since it is the time needed to take spin-down to spin-up which would be the state the furthest from our initial state. A comparison of the plots for different N reveals that when N is small, the infidelity is optimized at times that are odd multiples of $\frac{\pi}{\Omega}$. This can be understood because at even multiples of $\frac{\pi}{\Omega}$ we are essentially rotating back to spin-down. To ensure that the infidelity can be optimized for all time greater than the QSL, many pulses have to be applied. It is also interesting to note that even though it is known that any rotation can be decomposed into three rotations about orthogonal axes according to the Euler Decomposition, our studies for $N = 2$ suggests that any rotation can actually be decomposed into two rotations by the same angle about axes orthogonal to the initial or target state. We presume that this can be proven analytically.

We expand this study to systems with a general spin $j > 1/2$. A controllable Hamiltonian for a system with a larger Hilbert Space requires a term other than the angular momentum operators [17]. This is motivated with arguments related to the dimension of the Lie Algebra. In addition, a method of uniformly producing random target states in d- dimensional ($d = 2j + 1$) Hilbert Space

according according to the Haar measure on the Lie Group $SU(2)$ is discussed [19, 24]. With a controllable Hamiltonian and a method for generating random target states, we created plots like those for the case of spin-1/2 and noticed similarities. The QSL seems to be preserved for all N per dimension of the Hilbert Space within a window of $\frac{\pi}{\Omega}$. In addition, the curve of infidelity versus total time flattens for times greater than the QSL as the number of pulses N is increased.

There is still room for exploration of this problem. Something that could be investigated is the effect on controllability of the ratio of Ω and κ in the Hamiltonian for spins greater than 1/2. In this project, we assumed them to be equal but it could be that by changing how they compare we will get different dynamics that can change controllability of the system. The proof of Conjecture 2.4.1 is something that could potentially be proven analytically.

Overall, these results are interesting because they improve our intuition as to how resources necessary for quantum optimal control scale with dimension and see how to achieve "Pareto efficiency" in the context of control [5]. Having an understanding of what the best choices for control parameters are can assist when designing control protocols. The development of new quantum technologies has demanded a search for control protocols that are scalable, resourceful and robust. In particular, this is true for quantum computing where optimal control is often involved in control protocols for implementing unitary transformations [23, 20].

APPENDIX A

QUANTUM MECHANICS REVIEW

The matrix representation of the Pauli operators:

$$\hat{\sigma}_x = \begin{pmatrix} 0 & 1 \\ 1 & 0 \end{pmatrix} \quad \hat{\sigma}_y = \begin{pmatrix} 0 & -i \\ i & 0 \end{pmatrix} \quad \hat{\sigma}_z = \begin{pmatrix} 1 & 0 \\ 0 & -1 \end{pmatrix} \tag{A.1}$$

Any unitary operator of SU(2) can be written as an exponential $e^{-i\frac{\theta}{2}\hat{\vec{\sigma}}\cdot\vec{n}}$. Since there is a close relationship between SU(2) and SO(3), then it is equivalent to a rotation in $\mathbb{R}^3$ of angle θ about the unit vector $\vec{n}$:

$$R_{\vec{n}}(\theta) = e^{-i\frac{\theta}{2}\hat{\vec{\sigma}}\cdot\vec{n}} \tag{A.2}$$

A simple way of writing a unitary of SU(2):

$$e^{-i\frac{\theta}{2}\hat{\vec{\sigma}}\cdot\vec{n}} = \cos(\theta)\mathbb{1} - i\sin(\theta)\hat{\vec{\sigma}}\cdot\vec{n} \tag{A.3}$$

Angular momentum operators in the x and y directions can be expressed in terms of raising ($\hat{J}_+$) and Lowering ($\hat{J}_+$) operators.

$$\hat{J}_x = \frac{\hat{J}_+ + \hat{J}_-}{2} \tag{A.4}$$

$$\hat{J}_y = \frac{\hat{J}_+ - \hat{J}_-}{2i} \qquad \langle n|\,\hat{J}_y\,|m\rangle = \delta_{n,m}m \tag{A.5}$$

The eigenstates of the raising and lowering operators are:

$$\hat{J}_+ |j, m\rangle = \sqrt{j(j+1) - m(m+1)}\, |j, m+1\rangle = \alpha_m^+ |j, m+1\rangle \qquad (\text{A.6})$$

$$\hat{J}_- |j, m\rangle = \sqrt{j(j+1) - m(m-1)}\, |j, m-1\rangle = \alpha_m^- |j, m-1\rangle \qquad (\text{A.7})$$

Matrix representation of the raising and lowering operators:

$$\hat{J}_+ = \begin{pmatrix} 0 & \alpha_{j-1}^+ & 0 & \ldots & 0 \\ 0 & 0 & \alpha_{j-2}^+ & \ldots & 0 \\ \vdots & \ddots & & & \\ 0 & 0 & 0 & \ldots & \alpha_{-j}^+ \\ 0 & 0 & 0 & \ldots & 0 \end{pmatrix} \qquad \hat{J}_- = \begin{pmatrix} 0 & 0 & 0 & \ldots & 0 & 0 \\ \alpha_j^- & 0 & 0 & \ldots & 0 & 0 \\ 0 & \alpha_{j-1}^- & 0 & \ldots & 0 & 0 \\ \vdots & & \ddots & & & \\ 0 & 0 & 0 & \ldots & \alpha_{1-j}^- & 0 \end{pmatrix} \qquad (\text{A.8})$$

BIBLIOGRAPHY

[1] BE Anderson, H Sosa-Martinez, CA Riofrío, Ivan H Deutsch, and Poul S Jessen. Accurate and robust unitary transformations of a high-dimensional quantum system. *Physical review letters*, 114(24):240401, 2015.

[2] Neculai Andrei. Modern control theory. *Studies in Informatics and Control*, 15(1):51, 2006.

[3] Constantin Brif, Raj Chakrabarti, and Herschel Rabitz. Control of quantum phenomena: past, present and future. *New Journal of Physics*, 12(7):075008, 2010.

[4] Andres L Mora Carpio and Jorge I Mora. Ventilator management. In *Stat-Pearls [Internet]*. StatPearls Publishing, 2019.

[5] J. Chappelow. Pareto efficiency. Investopedia, 09 2019.

[6] Steven Chu. Cold atoms and quantum control. *Nature*, 416(6877):206–210, 2002.

[7] Domenico D'Alessandro. *Introduction to Quantum Control and Dynamics*. Taylor Francis Group, LLC, 2008.

[8] Sebastian Deffner and Eric Lutz. Quantum speed limit for non-markovian dynamics. *Physical Review Letters*, 111(1), Jul 2013.

[9] I.H. Deutsch. Physics 566 fall 2019 quantum optics, 2019.

[10] Roger Fletcher. *Practical methods of optimization*. John Wiley & Sons, 2013.

[11] John B. Fraleigh and Raymond A. Beauregard. *Linear Algebra, 3rd Edition*. Pearson, 3 edition, 1995.

[12] Navin Khaneja, Timo Reiss, Cindie Kehlet, Thomas Schulte-Herbrüggen, and Steffen J Glaser. Optimal control of coupled spin dynamics: design of nmr pulse sequences by gradient ascent algorithms. *Journal of magnetic resonance*, 172(2):296–305, 2005.

[13] Ronnie Kosloff, Stuart A Rice, Pier Gaspard, Sam Tersigni, and DJ Tannor. Wavepacket dancing: Achieving chemical selectivity by shaping light pulses. *Chemical Physics*, 139(1):201–220, 1989.

[14] VF Krotov and IN Feldman. An iterative method for solving optimal-control problems. *Engineering cybernetics*, 21(2):123–130, 1983.

[15] Adrian S Lewis and Michael L Overton. Nonsmooth optimization via bfgs. *Submitted to SIAM J. Optimiz*, pages 1–35, 2009.

[16] L. Mandelstam and Ig. Tamm. *The Uncertainty Relation Between Energy and Time in Non-relativistic Quantum Mechanics*, pages 115–123. Springer Berlin Heidelberg, Berlin, Heidelberg, 1991.

[17] Seth Merkel. *Quantum Control of d-Dimensional Quantum Systems with Application toAlkali Atomic Spins*. PhD thesis, The University of New Mexico, 06 2009.

[18] R Nigmatullin and SG Schirmer. Implementation of fault-tolerant quantum logic gates via optimal control. *New Journal of Physics*, 11(10):105032, 2009.

[19] M. Ozols. How to generate a random unitary matrix, 03 2009.

[20] José P Palao and Ronnie Kosloff. Quantum computing by an optimal control algorithm for unitary transformations. *Physical review letters*, 89(18):188301, 2002.

[21] P. M. Poggi, F. C. Lombardo, and D. A. Wisniacki. Time-optimal control fields for quantum systems with multiple avoided crossings. *Physical Review A*, 92(5), Nov 2015.

[22] D.B. Westra. Su(2) and so(3). Notes, 2 2008.

[23] Frank K Wilhelm, Susanna Kirchhoff, Shai Machnes, Nicolas Wittler, and Dominique Sugny. An introduction into optimal control for quantum technologies. *arXiv preprint arXiv:2003.10132*, 2020.

[24] Karol Zyczkowski and Marek Kus. Random unitary matrices. *Journal of Physics A: Mathematical and General*, 27(12):4235, 1994.